EXPERIMENTAL INVESTIGATION OF THE ACOUSTIC SIGNATURE OF A QUAD-ROTOR EVTOL AIRCRAFT IN HOVER

Gemma Bucherelli, Luyiza Das, Donato Grassi, Daniele Granata, Alex Zanotti
Politecnico di Milano, Dipartimento di Scienze e Tecnologie Aerospaziali, via La Masa 34, 20156, Milan, Italy

ABSTRACT

The present study aims at providing a proper aeroacoustic characterization of the single-passenger configuration of the quadrotor concept vehicle designed by NASA, through an experimental campaign in the new anechoic chamber at Politecnico di Milano. A scaled model of the quadrotor CRM was designed from scratch and manufactured to be exploited to collect aerodynamic force and acoustic measurements in hover condition, with a particular focus on rotor-on-rotor interaction phenomena by adopting a breakdown approach where rotors were progressively added.

NOTATION

A = rotor disk area $[m^2]$
BPF = blade passing frequency $[Hz]$
c = blade chord $[m]$
C_{F_i} = global force coefficient $= F_i/(\rho A\omega^2R^2)$ [-]
C_{M_i} = global moment coefficient $= M_i/(\rho A\omega^2R^3)$ [-]
C_T = rotor thrust coefficient $= T/(\rho A\omega^2R^2)$ [-]
C_Q = rotor torque coefficient $= Q/(\rho A\omega^2R^3)$ [-]
d_x = longitudinal distance of master rotor axis $[m]$
d_y = lateral distance of master rotor axis $[m]$
d_z = vertical distance of master rotor axis $[m]$
f_s = sampling frequency $[Hz]$
F_x = global longitudinal force $[N]$
F_y = global lateral force $[N]$
F_z = global vertical force $[N]$
H = fuselage height from the floor $[m]$
l_x = longitudinal distance of master rotor axis from microphone arc center $[m]$
M_x = global rolling moment $[Nm]$
M_y = global pitching moment $[Nm]$
M_z = global yawing force $[Nm]$
ρ = air density $[kg/m^3]$
Q = rotor torque $[Nm]$
$OASPL$ = Overall Sound Pressure Level [dB]
PSD = Power Spectral Density $[\frac{m/s^2}{Hz}]$
R = rotor radius [m] R_m = microphone arc radius [m]
s = fiselage width [m]
SPL = Sound Pressure Level [dB]
T = rotor thrust [N]
γ = angular coordinate of microphones $[deg]$
Φ = angular step between microphones $[deg]$
ω = rotor angular velocity $[rad/s]$

INTRODUCTION

The process of rapid urbanization combined with the growing population density and pollution are leading to constant increase in mobility needs (Ref. 1). Urban Air Mobility (UAM) is an emerging air transportation system made possible by advanced technologies (Ref. 2). In this promising field a particular focus has recently been addressed to electric vertical take-off and landing (eVTOL) aircraft with unconventional designs, including side-by-side or tandem configurations and layouts combining multiple wings. These disruptive concepts introduce new challenges in every aspect of the design process. In particular from an aerodynamic standpoint they present several interactional phenomena, that directly affect the aircraft performances, handling qualities and particularly noise generation. Indeed, noise is perceived in the literature and by experts as a predominant risk of UAM, as the entry-into-service of urban aerial vehicles would imply an increase of urban acoustic pollution due to the low altitude flight and frequent landing/take-off operations in the vertiport sites. Thus, noise pollution is increasingly becoming an environmental concern and an influencing factor of the citizen quality of life and well-being. The World Health Organization (WHO, Geneva, Switzerland) lists several adverse health effects known for aviation noise, strongly recommending that noise levels do not exceed 45 dB Lden during the daytime and 40 dB Lnight during the night. Consequently, UAM aircraft must be significantly quieter than today's helicopters to be acceptable, which poses a major challenge in aircraft design. As noted by Straubinger et al. (Ref. 3), potential strategies for noise reduction include distributing thrust across multiple rotors, reducing take-off weight or increasing rotor area. However, the latter is in contrast with the need for air taxis to remain compact, given the limited space in cities. This means that aircraft size and seating capacity could become limiting factors for the throughput of vertiports in urban areas. In general all the previous considerations stress the urge for a proper characterization of the different eVTOL configurations in terms of acoustic footprint, eventually as a basis for an optimization process.

The present work was aimed at providing guidelines to address this goal, in particular improving knowledge about acoustic footprint of a quad-rotor eVTOL configuration, which is a unique type of VTOL aircraft allowing for centralization of the payload and control system. This configuration enables a wide range of alternatives for flight control and performance optimization and may be designed following different architectural choices, including hybrid, turbo-shaft and fully electric systems, as well as collective pitch control and RPM-based control strategies (Ref. 4). In the case of RPM controlled quad-rotor configurations, propellers may have fixed-pitch blades for a fixed flight condition, while their control in roll, pitch and yaw is achieved through the use of the throttle of each rotor (Ref. 5). The four rotors are typically aligned such that the ones on opposite ends rotate in the same direction and the other two in the reverse direction, this allows to balance the vehicle removing the need for a tail rotor. Thanks to their unique advantages with respect to traditional helicopters, including high maneuverability, compact size and ease of control, quad-rotors are promising to be used in a variety of applications also beyond UAM. Among these, search-and-rescue and emergency response are perhaps the most significant. Other major uses include homeland security, military surveillance and search-and-destroy operations (Ref. 6). Another important advantage of this configuration lies in considerably low disk-loading values, which is a typical characteristic of all multi-copters. Disk loading is a fundamental parameter for VTOL aircraft design, as it strongly affects performance and noise. In general, the lower the disk loading, the better the hover performance, which results in a reduction in power required to maintain hover flight (Ref. 7). Additionally, lower disk loading allows for quieter hover characteristics (Ref. 8), which constitutes an extremely important benefit as this kind of aircraft is typically characterized by a considerable noise impact due to the large number of rotors, that compromises its social acceptance. Given these advantages in hover condition, it is important to highlight that multi-copters are not optimized for cruise flight. Indeed, they present very low lift-to-drag ratios due to the absence of wings that implies that the rotors are used for both lift and thrust. This makes these aircraft better suited for short-range, low-speed applications, such as urban air taxi services (Ref. 9).

NASA's Revolutionary Vertical Lift Technology (RVLT) project is developing UAM VTOL aircraft designs that serve as focal points to guide research activities aimed at supporting aircraft development for emerging aviation markets. Among these aircraft configurations, NASA proposes a common reference model (CRM) of a quad-rotor concept described in (Refs. 4, 10, 11). This innovative VTOL aircraft configuration has already collected numerous studies that through numerical analyses have highlighted significant aerodynamic interaction effects across the flight envelope, which have a major impact on acoustic emissions (Ref. 12). The possibility to have several design parameters in terms of rotor size and positioning and fuselage geometry has demonstrated the need for further investigation, that is essential to achieve the optimization of this configuration. In particular, the present work was aimed at improving knowledge on these configurations, in particular by investigating the acoustic signature of the one-passenger RPM controlled NASA CRM quad-rotor configuration (see Fig. 1). The goal of the activity was to perform a comprehensive experimental activity aimed at characterizing the noise footprint related to the mutual aerodynamic interaction phenomena among rotors across the flight envelope conditions of this aircraft mission. In particular, in this study, preliminary results regarding the acoustic signature measured for hover conditions are presented and discussed.

Figure 1. Layout of the one-passenger NASA CRM electric quad-rotor configuration (Ref. 10).

EXPERIMENTAL SET-UP

Model design and equipment

A wind tunnel scaled model based on the NASA CRM quad-rotor geometry was designed from scratch and manufactured at Politecnico di Milano. The layout of the quad-rotor model is shown in Fig. 2. The scaling factor was set to 1:16.9, guaranteeing a span-to-span dimension around 0.5 m, in order to fit into the test chamber of the main facilities exploited at Aerodynamics Laboratory of the Department of Aerospace Science and Technology of Politecnico di Milano. The main geometrical characteristics of the scaled model are reported in Tab. 1.

Table 1. Main scaled model geometrical characteristics.

Disk radius [mm]	112
Number of blades	3
Coning angle [°]	1.7
L_x [mm]	303
L_y [mm]	303
L_z [mm]	40
l [mm]	252
s [mm]	77
h [mm]	89

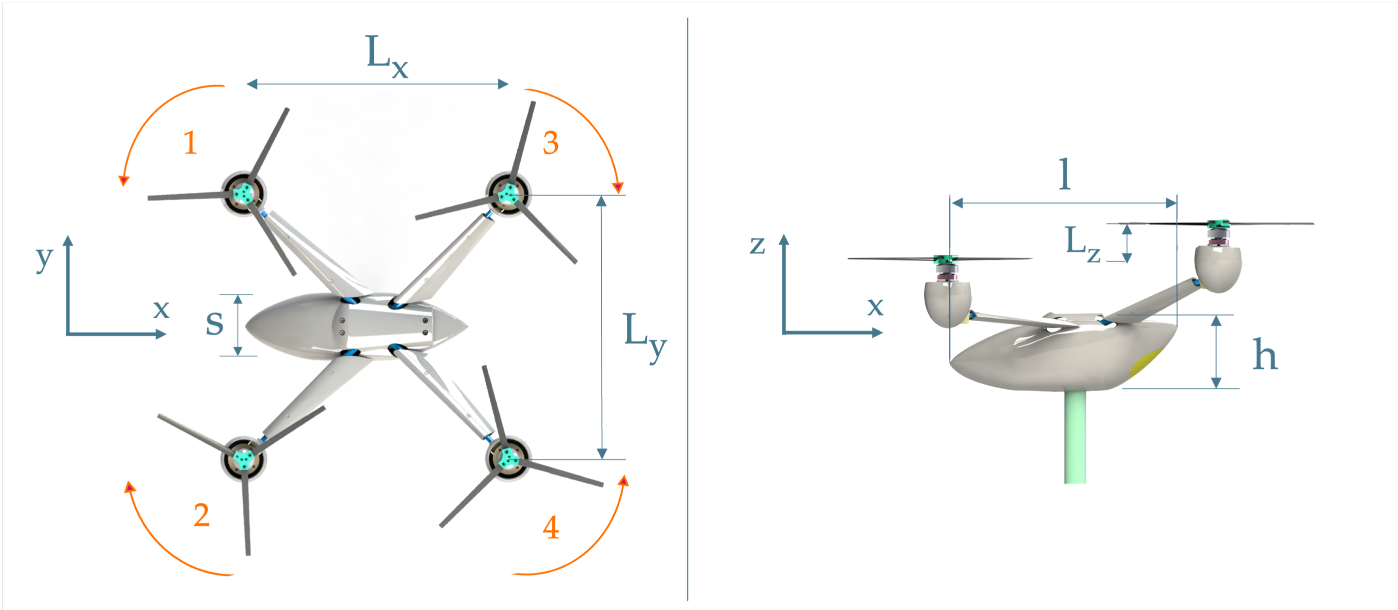

Figure 2. Layout of the quad-rotor scaled model.

The model was designed considering an internal metallic supporting structure in Ergal alloy composed by a system of plates attached to a vertical steel sting and housing an internal balance (see Fig. 3(a)). Four steel arms are used to connect the rotor hubs to this structure, each equipped with an electric motor and a couple of load cells for local thrust and torque measurements (see Fig. 3(b)). The whole internal structure was covered with a fuselage shell and fairings for the arms and the rotor hubs, that were obtained through rapid-prototyping technique, exploiting Windform 2.0, which is a composite 3D printing material reinforced with carbon fiber, that guarantees high mechanical properties. In order to allow for enough robustness and solid joints, the thickness throughout all the structures was maintained around 2 mm. The rotor blades were manufactured using carbon fiber to ensure the highest stiffness. Specifically, a unidirectional layer was used to withstand the centrifugal force, while two layers inclined at 45° were applied to resist the torsional moment.

The model is equipped with devices selected considering the expected loads and the extremely contained dimensions of the model, that was designed to house them. As previously stated, an internal balance was placed in the fuselage structure to measure the global forces and moments. In particular, a six-component miniature strain gauge balance ATI Mini40-E was selected due to its compact design. Each rotor hub is equipped with a miniaturized torsiometer Futek QTA141 and an axial load cell Burster 8432-5050 to respectively measure thrust and torque for each rotor, driven by a brushless BrotherHobby TC 2004 Ultralight motor. The main specifications of the motors, main balance, axial load cells and torsiometers are reported respectively in Tabs. 2, 3, 4, 5. In addition, each hub was equipped with an Hall effect sensor, placed sufficiently close to the corresponding motor, in order to measure its rotational speed. The sensor consists of two magnetic components: one represented by the motor itself and the other mounted on the nacelle. When these magnets are close to each other during each rotor revolution, they complete an electrical circuit. As a result, the sensor produces a voltage signal with spikes that occur each time the magnets align and close the circuit. By analyzing the frequency spectrum of this signal the rotational speed of the propeller can be determined. The model reference system is centered in the middle of the main balance, as reported in Fig. 4, highlighting also the main distances of the rotor disks.

Anechoic chamber

The model realized according to the design procedure previously described was employed to perform force and acoustic measurements in hover. This experimental campaign was conducted in the new anechoic test chamber of the Department of Aerospace Science and Technology (DAER) of Politecnico di Milano. This facility represents the plenum of the open-jet test chamber of a new aeroacoustic wind tunnel, which is still under construction (Ref. 13). The sizing of the chamber was obtained from a fair trade-off between space required for the lowest cut-off frequency possible and the actual room available in the building. In particular the usable internal region was set to $4m \times 4m \times 4m$, with an external size of $6.5m \times 6.5m \times 5.8m$. These values, considering the addition of sound-absorbing cones, result in a maximum cut-off frequency of 100 Hz. The external structure consists of three interconnected modules reinforced by a metallic cage. The central module features a lateral door to access the test region, facilitating model adjustments. The lateral modules are reinforced with tie rods to enhance stiffness and support the wedge addition, with openings designated for the future wind tunnel. To minimize acoustic reverberation, the chamber

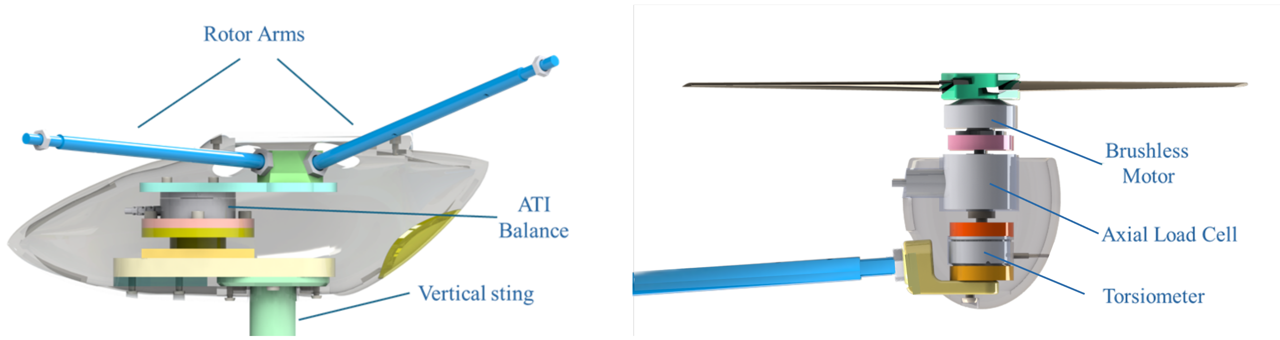

(a) Internal layout

(b) Detail of the rotor hub

Figure 3. Internal layout of the quad-rotor experimental model.

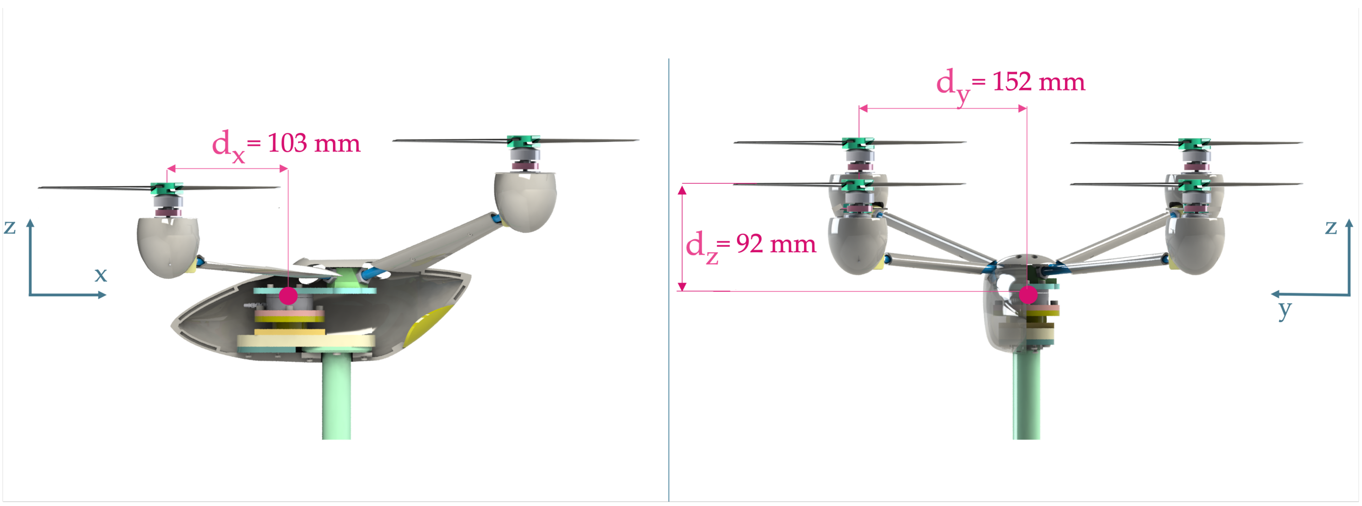

Figure 4. Definition of the reference system for force measurements.

Table 2. Main specifications of the BrotherHobby TC 2004 Ultralight Motor.

Dimensions [mm]	kV	Voltage [V]	Max Current [A]	RPM
24.6 ⌀× 17.4	1700	24	14.1	26341

Table 3. Main specifications of the Force/Torque sensor ATI Mini40-E SI-80-4.

Dimensions [mm]	F_x [N]	F_y [N]	F_z [N]	M_x [Nm]	M_y [Nm]	M_z [Nm]
40 ⌀× 12.2	80	80	240	4	4	4

Table 4. Main specifications of Burster Precision Miniature Tension and Compression Load Cell 8432 5050.

Dimensions [mm]	T_z [N]
25.4 ⌀× 21.9	50

Table 5. Main specifications of the Futek QTA141 Micro Reaction Torque Sensor.

Dimensions [mm]	M_z [Nm]
22 ⌀× 10	1

walls are covered with anechoic wedges, that follow a pattern where two sets of orthogonally positioned wedges improve noise refraction, directing sound waves along a mazelike path to enhance interaction with the absorbing material. Additionally, the lateral door's internal surface is lined with the same material to prevent external noise infiltration.

The model was placed in the middle of the described chamber (see Fig. 5) in order to ensure acoustic symmetry and minimize residual reflections from the walls. The acoustic set-up is presented in the scheme shown in Fig. 6. An axisymmetric pylon was engaged to support the vertical sting and a metallic arc was placed above the model at midspan section of the chamber aligned with the longitudinal direction, housing an array of eleven microphones fixed equally spaced. Both these metallic structures were covered with noise absorbing material in order to minimize reverberation effects.

Figure 5. Quad-rotor model set up in the anechoic test chamber.

EXPERIMENTAL RESULTS

The experimental campaign was performed in order to evaluate the effects of the mutual interaction between the rotors on the aerodynamic loads and on the acoustic signature of the model, in particular focusing on a specific flight condition with all the rotors rotating at 6900 RPM. With this aim, measurements were performed using a breakdown approach, starting from a single rotor configuration, considered as master, thus adding the other ones, while the fuselage shell and fairings were maintained in position for all the different configurations, in order to enclose and cover cables. In particular, both a side-by-side and a tandem rotor configuration were considered, respectively activating the second and the third rotor together with the master one, finally the whole model was tested. A further analysis was conducted keeping the front rotors' rotational speed at 6900 RPM and adapting the rear rotors' one (i.e at 5300 RPM) in order to achieve a longitudinally trimmed condition for the pitching moment, thus resembling a more realistic flight condition in hover for the vehicle (Refs. 5, 14) to be compared in particular in terms of acoustic signature. The different configurations analyzed in the test matrix are summarized in Tab. 6. The instrumentation embedded in the model enabled to evaluate the quad-rotor integral loads as well as the partial loads acting on each rotor. In parallel with load measurements, the acoustic footprint at microphones positions was also measured.

Table 6. Test matrix (rotors numbered according to Fig. 2).

Configuration	Rotors	front RPM	rear RPM
ISO-ROT1	1	6900	6900
SBS	1, 2	6900	6900
TND	1, 3	6900	6900
4ROTs	1, 2, 3, 4	6900	6900
4ROTs-T	1, 2, 3, 4	6900	5300

Force measurements

In order to verify the repeatability of the force measurements, multiple runs were conducted for the ISO-ROT1 configuration. Table 7 shows the standard deviations of the aerodynamic coefficients evaluated over 8 different runs for both the main balance and the master rotor load cells. As can be observed, the quite small values of the standard deviation of the coefficients confirms the quite good repeatability of the measurements. Once the repeatability check was provided, force measurements were conducted considering the different configurations from Table 6. Histograms in Figure 7 summarize the results obtained in terms of global thrust and pitching moment from the main balance across the different configurations. Figure 7(a) shows how increasing the number of rotors leads to an expected linear growth in global thrust. In particular, the SBS and TND configurations provide almost the same thrust. Figure 7(b) shows an increasing positive pitching moment between the single and side-by-side rotors configuration. On the other hand, as the position of the main balance is not symmetrical with respect to the front and rear rotors, i.e closer to front rotors, this produces a non negligible negative pitching moment both in the tandem and complete configurations, thus the model appears non trimmed for this hover condition with respect to pitch axis.

Moving to the results in terms of non dimensional local loads detected on each rotor, Figure 8 shows the slight differences between both C_T and C_Q values referring to the same rotor across the four configurations and contained discrepancies among all in general. This allows to confirm the coherent behavior of the different components of the model. Figure 9 compares the global thrust and pitching moment for the complete model in 4ROTs and 4ROTs-T conditions. In particular, the comparison of the global pitching moment shown in Fig. 9(b) confirms that in 4ROTs-T the different RPM between the front and rear rotors resembles a quite longitudinally trimmed condition in hover for the complete model. The reduction in thrust observed for the trimmed configuration in Fig. 9(a) is expected due to the decrease of rear rotors rotational speed.

Acoustic measurements

Acoustic measurements were post-processed from the time histories of the microphones' signals through the analysis of the Power Spectral Density (PSD), the Overall Averaged Sound Pressure Level (OASPL), and the SPL spectra. These analyses provide insights into the distribution of acoustic in-

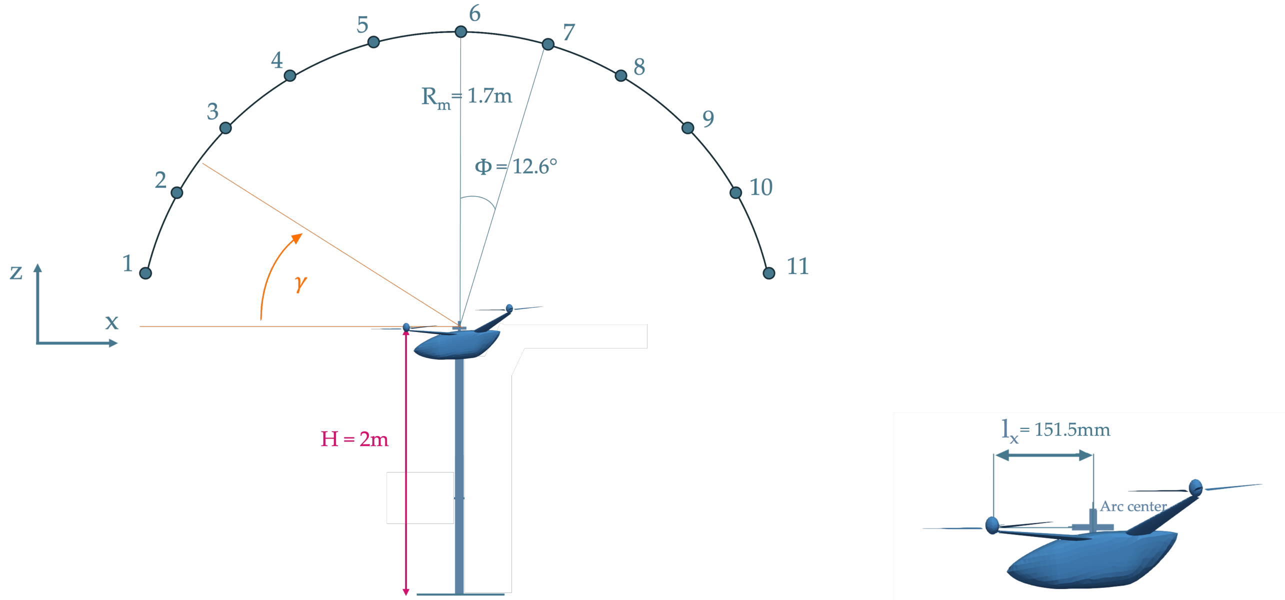

(a) Microphone scheme

(b) Microphone scheme detail

Figure 6. Acoustic measurements set-up.

Table 7. Standard deviations of force and moment coefficients from axial load cell, torque sensor and main balance respectively in the ISO-ROT1 configuration.

σ_{C_T}	σ_{C_Q}	$\sigma_{C_{F_x}}$	$\sigma_{C_{F_y}}$	$\sigma_{C_{F_z}}$	$\sigma_{C_{M_x}}$	$\sigma_{C_{M_y}}$	$\sigma_{C_{M_z}}$
4.3748×10^{-5}	6.2907×10^{-6}	4.4245×10^{-6}	1.5156×10^{-5}	2.9517×10^{-5}	3.9893×10^{-5}	3.1470×10^{-5}	5.1434×10^{-6}

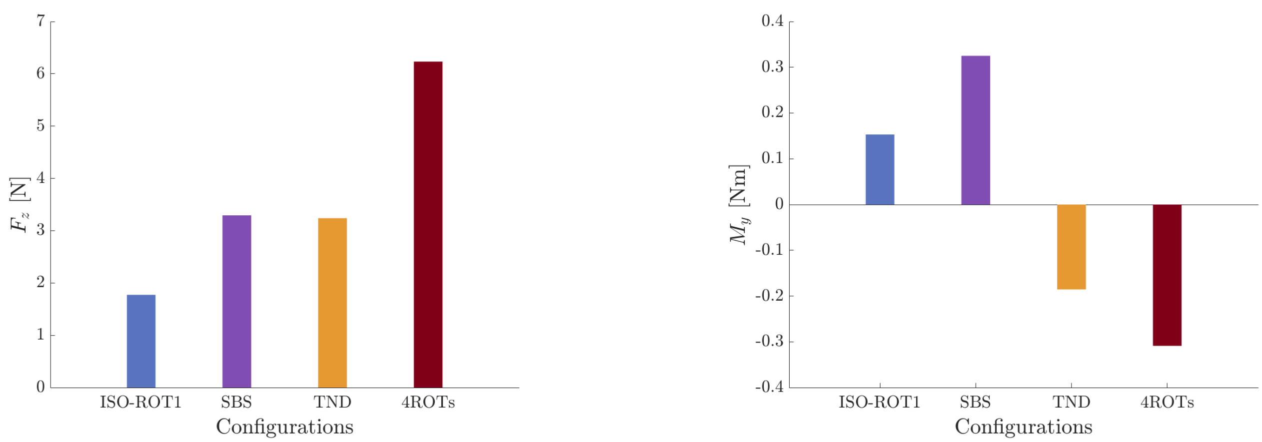

(a) F_z from main balance

(b) M_y from main balance

Figure 7. Load measurements from the main balance across different configurations.

tensity in the frequency domain. Before illustrating the acoustic results the presence of recirculation effects in the anechoic test chamber was investigated. Several aeroacoustic studies conducted on rotors and propellers in anechoic chambers (Refs. 15, 16) have observed this phenomenon, that consists in wide thrust fluctuations occurring once the flow stabilizes within the chamber. This leads to an increase in both harmonic and broadband noise, that appears as a sequential amplification in correspondence of the BPFs, especially in higher order ones. To prevent misleading results, it is crucial to take measurements before recirculation starts and after the rotor loads have stabilized. The occurring of recirculation is

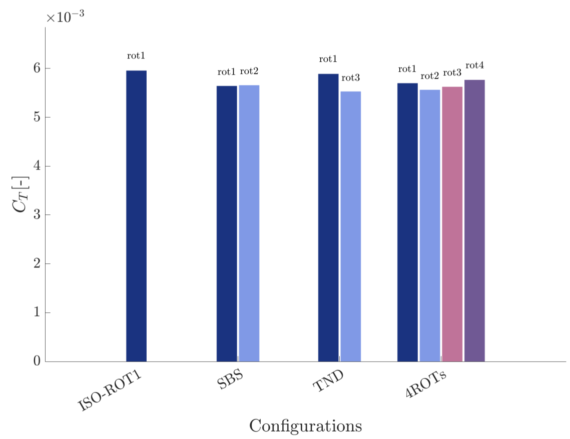

(a) C_T from each axial load cell

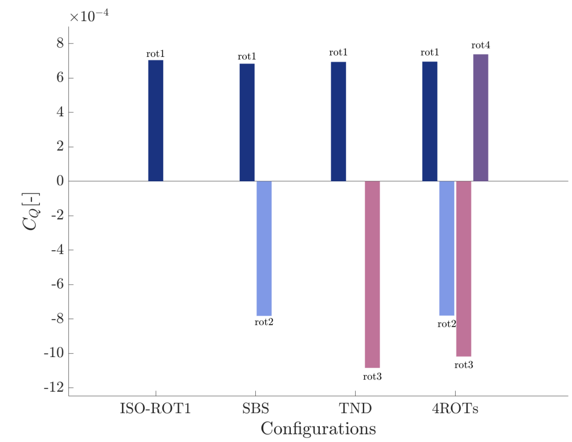

(b) C_Q from each torque sensor

Figure 8. Load measurements from each rotor load cell across different configurations.

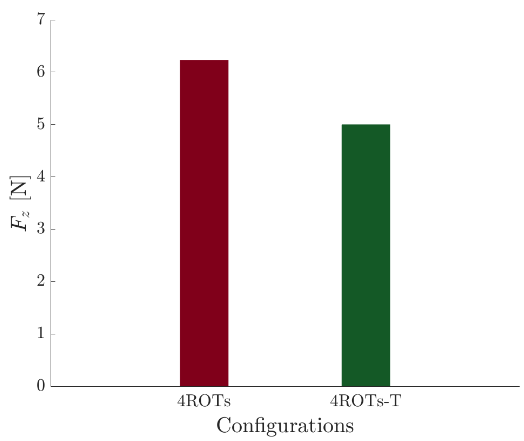

(a) F_z from main balance

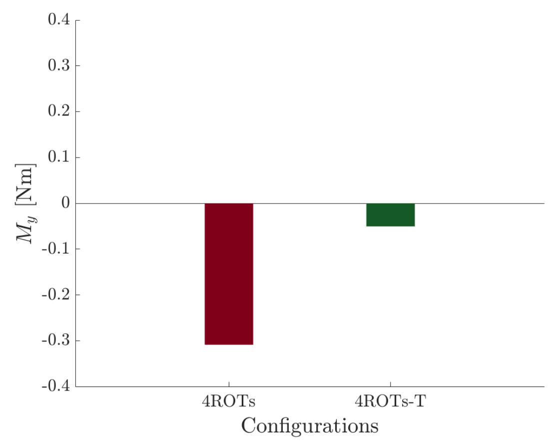

(b) M_y from main balance

Figure 9. Load measurements from the main balance: comparison between 4ROTs and 4ROTs-T (trimmed).

influenced by factors such as rotor geometry, test equipment, and the size of the chamber (Refs. 15, 16). An estimation of the recirculation effects for the present experimental set up was retrieved from the microphone 6 signal acquired for the 4ROTs configuration, considered the most critical one. Figure 10 shows the spectrogram of microphone 6 signal along the acquisition time of 8 seconds. This representation shows how peaks in correspondence of the BPFs keep their SPL amplitude throughout the acquisition time, thus not showing recirculation effects related to the four rotors.

In analogy with the approach followed for the force measurements, a repeatability check was conducted for the microphones measurements considering the results obtained from 8 runs performed for the ISO-ROT1 configuration. Figure 11 shows the mean OASPL obtained from the repeated runs plotted in the Cartesian plane along with the standard deviations values depicted as errorbars. The quite low values of the OASPL standard deviations proves a good repeatability of the acoustic measurements. Thus, in order to enhance the readability of the results, in the following OASPL plots the error bars due the quite small variability of acoustic measurements across different runs are not represented.

Figure 12 shows a progressively increasing noise impact as the number of rotors grows, with the maximum OASPL in correspondence of the sixth microphone ranging from around 64 dB for the ISO-ROT1 configuration to 71 dB for the whole model. It is particularly interesting to notice that, conversely to what was observed in terms of the global thrust generated, the two configurations including a couple of rotors show a different acoustic behavior. In particular, the SBS configuration produces a more consistent noise signature with respect to the TND one, with a 2 dB increase in correspondence of the sixth microphone. In order to further investigate the comparison between these two configurations also the SPL specra obtained

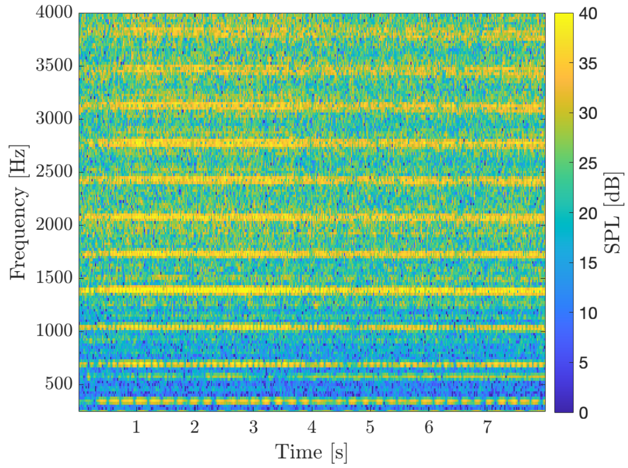

Figure 10. Spectrogram of microphone 6 signal for 4ROTs configuration.

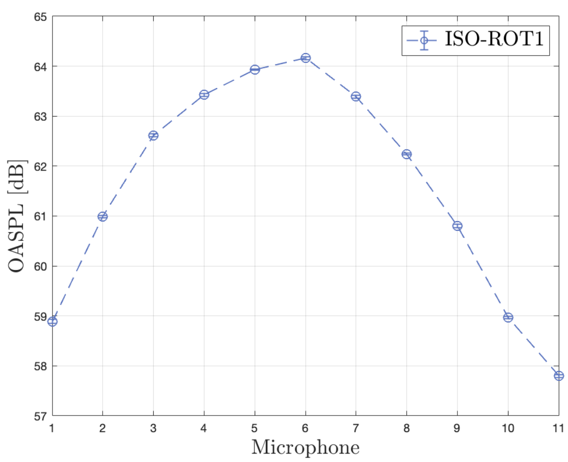

Figure 11. Microphones measurements repeatability: mean OASPL and standard deviations for ISO-ROT1 configuration.

from signals detected by the sixth microphone are shown in Fig. 13(a). The peaks in correspondence of the blade passing frequency and its integer multiples (BPFs) can be easily identified. In particular, they appear to be higher for the SBS case, which confirms the stronger noise signature of this latter configuration. Beside these expected frequencies, also harmonics at every $(2k-1)BPF/3$ are highlighted, where k is an integer in the range $[1,+\infty)$. They are generally defined as *sub-harmonics* and their presence in the SPL spectra was also observed in literature for a similar propeller test case (Ref. 17) and attributed to a noise component given by the geometrical dissimilarities of each rotor's blades, as shown in (Ref. 18). However the differences between the two configurations in correspondence of the sub-harmonics and along the other frequencies appear less appreciable from this graph with respect to the gaps in correspondence of BPFs. These discrepancies could be attributed to a higher intensity of pressure fluctuations on the rotor disk experienced in the SBS case due a more robust interaction. It appears that, even if the model four rotors are equidistant from the floor point of view, the vertical offset between the front and rear rotor couples, which comes into play only in the TND configuration, reduces interaction phenomena with respect to the SBS one, characterized by coplanar rotors.

A final analysis involved the broadband noise component, which is generally due to the interaction of rotor blades with turbulence and results in random blade loading variations (Ref. 19). This contribution is particularly relevant for highly turbulent flows, such as those encountered in rotor analysis in the presence of overlapped disk configurations (Ref. 20). Although the hover conditions analyzed in the present study are expected to present limited interaction phenomena, the rotor wakes interact with the fuselage body for all the configurations, surely generating a non-periodic broadband noise. This pressure perturbation contributes to the SPL spectra in the form of low random fluctuations distributed over different frequencies. Figure 13(b) shows the SPL spectra referring to the sixth microphone with the broadband noise highlighted for the SBS and TND configurations. To better appreciate the contribution of broadband noise, a least-squares interpolation on the SPL spectrum curve was performed at points between the multiples of the BPF, as was similarly done by Zawodny et al. (Ref. 21) to avoid tonal contributions. This approach isolates the frequency trend caused by tonal frequencies from that of background noise, which is distributed across all frequencies. The slightly higher contribution in the SBS configuration suggests that also the broadband noise contributes in identifying this configuration as the most impactful between the two in terms of noise generation, meaning the turbulence level is higher with respect to the TND case. However the discrepancy between the two configurations appears lighter compared to the considerable gap encountered comparing the tonal noise peaks.

The same approach of investigation in terms of acoustic results was conducted also to compare the simplest and the most complex configurations, i.e. ISO-ROT1 and 4ROTs, that appear at the opposite extremes of the OASPL plot from Figure 12. The strong difference encountered for the OASPL values is also encountered in both plots presented in Fig. 14. Discrepancies in the SPL spectra are particularly visible in correspondence of the BPFs tonal peaks, associated to the aerodynamic loads that present a considerable increase (see Fig. 14(a)). The broadband contribution shown in Fig. 14(b) proves the increase in turbulence level due to the introduction of multiple rotors.

A final analysis concerned the comparison in terms of acoustic signature encountered between the complete configurations at constant rotors RPM and in longitudinally trimmed condition (4ROTs-T) was therefore performed. Figure 15 shows the OASPL across the 11 microphones for the 4ROTs-T configuration compared to the 4ROTs one. As expected, the reduction in the rear components' rotational speed impacts on the noise produced, with a decrease of the maximum value

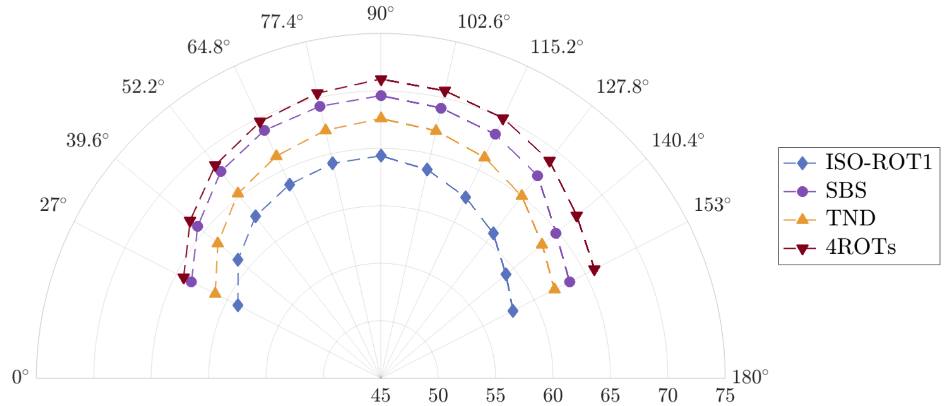

Figure 12. Comparison of OASPL for the different configurations.

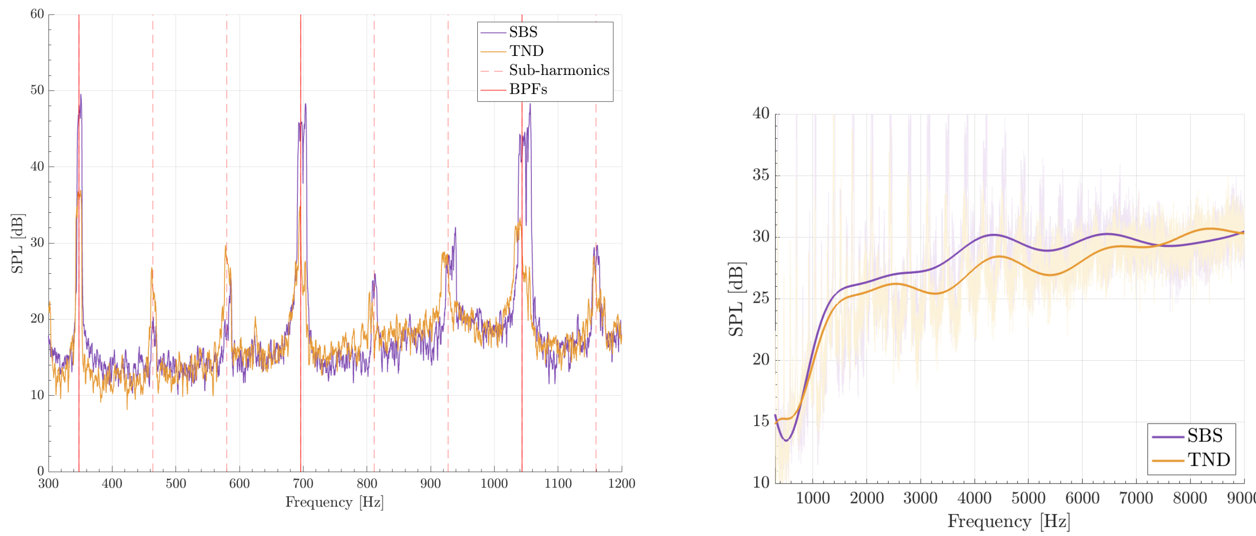

(a) SPL spectra (mic 6), sub-harmonics (dashed lines) and BPFs (continuous lines).

(b) Broadband noise contribution (mic 6).

Figure 13. Acoustic measurements comparison: SBS vs TND configurations.

(sixth microphone) of about 2.5 dB. For a further investigation in Fig.16 the SPL spectra and the broadband noise component in the two cases are compared, showing how this discrepancy is confirmed both in terms of tonal peaks and of the turbulence-associated fluctuations (broadband noise contribution) distributed a wider spectrum of frequencies.

CONCLUSIONS

The aerodynamic and acoustic characterization in hover of the single-passenger quadrotor concept vehicle designed by NASA was provided through an experimental campaign. The objective was to address the lack of literature on this configuration, which was analyzed in past works only from a numerical point of view. In addition this study focuses on the investigation of rotor-on-rotor interaction phenomena, that, among the various technological challenges associated with eVTOLs, represents one of the most critical aspects for their aerodynamic performance and acoustic signature, thus compromising their successful entry-into-service. In the following the main goals of the activity.

1. A scaled model of the quadrotor CRM was designed from scratch and manufactured in order to be exploited for wind tunnel testing. The most critical aspect consisted in the materials and the devices choice considering the extremely contained dimensions of the model, dictated by the size of the facilities in use.
2. The recently built anechoic chamber at Politecnico di Milano was exploited for the first time allowing to conduct a first experimental campaign coupling force and acoustic measurements.
3. Adopting a breakdown approach with a progressive addition of active rotors allowed to investigate the impact of interaction effects both on the loads generated and on the

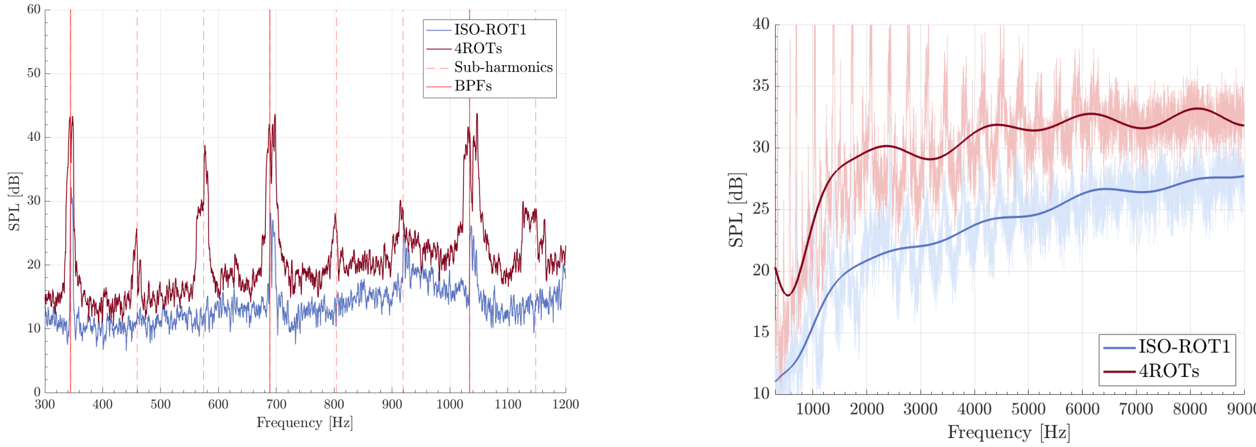

(a) SPL spectra (mic 6), sub-harmonics (dashed lines) and BPFs (continuous lines).

(b) Broadband noise contribution (mic 6).

Figure 14. Acoustic measurements comparison: ISO-ROT1 vs 4ROTs configurations.

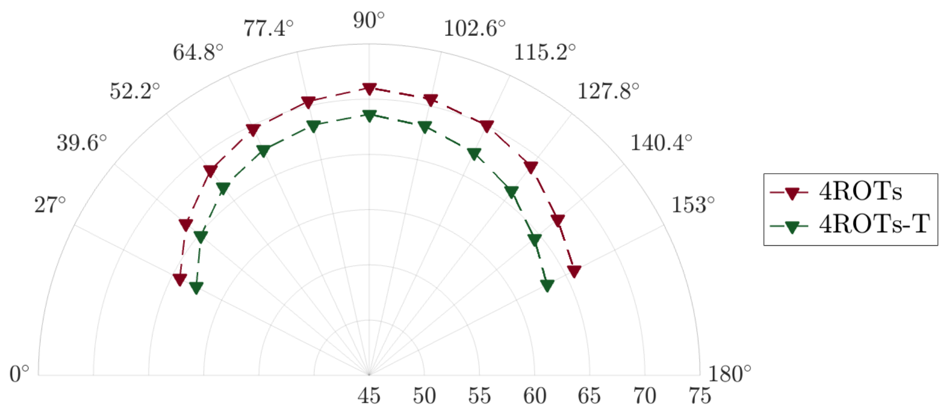

Figure 15. Comparison of OASPL between 4ROTs and 4ROTs-T configurations.

noise footprint. Increasing the number of components all equally rotating at 6900 RPM results in an expected increase in the global thrust, with two rotors in side-by-side and tandem configurations showing a similar behavior. Moreover, a longitudinally trimmed condition was tested by varying the rear rotors ROM in order to evaluate the acoustic impact of a more realistic flight condition for the vehicle.

4. Acoustic measurements allowed to appreciate the increasing OASPL as the complexity of the configuration grows. It is particularly interesting to observe how the two rotors in side-by-side and tandem configurations show a considerable discrepancy, visible also in the tonal and broadband noise contributions. This could be related to the higher intensity of pressure fluctuations experienced by the blades in the SBS case due to the coplanarity of the rotors involved, opposed to the vertical offset present in the TND configuration. For what concerns the whole model, moving from the configuration with all the components equally rotating at 6900 RPM to the longitudinally trimmed one leads to a reduction in the acoustic impact, immediately appreciable from the OASPL comparison, reflected also in the SPL spectra tonal peaks and in the broadband noise contribution.

Future development of the activity will be focused on the experimental aerodynamic and aeroacoustic characterization of the quad-rotor model also in cruise flight conditions, by performing loads and microphone measurements in the new built anechoic wind tunnel.

Author contacts:
Gemma Bucherelli, gemma.bucherelli@polimi.it
Luyiza Das, luyiza.das@polimi.it
Donato Grassi, donato.grassi@polimi.it
Alex Zanotti, alex.zanotti@polimi.it

ACKNOWLEDGMENTS

The work in this study was carried out within the MOST -— Sustainable Mobility National Research Center and received

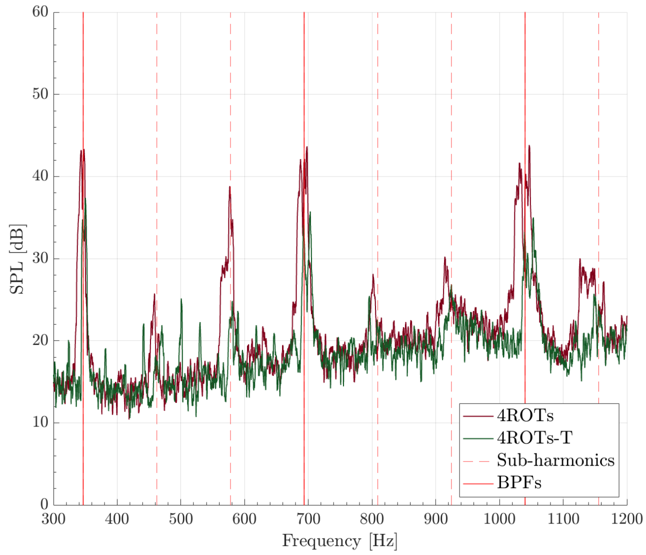

(a) SPL spectra (mic 6), sub-harmonics (dashed lines) and BPFs (continuous lines).

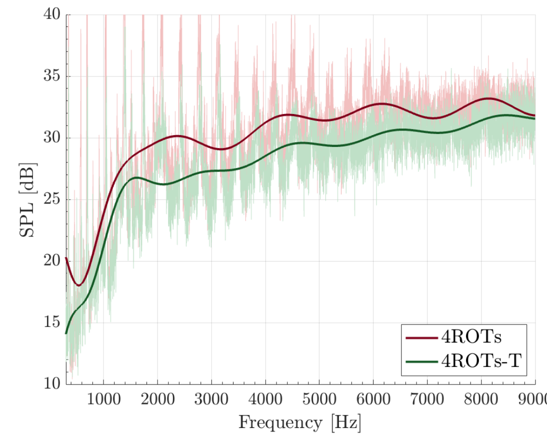

(b) Broadband noise contribution (mic 6).

Figure 16. Acoustic measurements comparison: 4ROTs vs 4ROTs-T configurations.

funding from the European Union Next-Generation EU (PIANO NAZIONALE DI RIPRESA E RESILIENZA (PNRR) – MISSIONE 4 COMPONENTE 2, INVESTIMENTO 1.4 – D.D. 1033 17/06/2022, CN00000023). This manuscript reflects only the authors' views and opinions, neither the European Union nor the European Commission can be considered responsible for them.

CENTRO NAZIONALE PER LA MOBILITÀ SOSTENIBILE

REFERENCES

1. Pavan Yedavalli. An assessment of public perception of urban air mobility (uam). 2020.

2. H. Pak. Can urban air mobility become reality? opportunities and challenges of uam as innovative mode of transport and dlr contribution to ongoing research. *CEAS Aeronautical Journal*, 2024. Published online on May 7, 2024.

3. Straubinger et al. An overview of current research and developments in urban air mobility – setting the scene for uam introduction. *Journal of Air Transport Management*, 87:101852, 2020.

4. W. Johnson and C. Silva. Nasa concept vehicles and the engineering of advanced air mobility aircraft. *The Aeronautical Journal*, 126:1–33, 10 2021.

5. Wayne Johnson, Christopher Silva, and Eduardo Solis. Concept vehicles for vtol air taxi operations. In *AHS Specialists"Conference on Aeromechanics Design for Transformative Vertical Flight*, number ARC-E-DAA-TN50731, 2018.

6. Shweta Gupte, Paul Infant Teenu Mohandas, and James M. Conrad. A survey of quadrotor unmanned aerial vehicles. *2012 Proceedings of IEEE Southeastcon*, pages 1–6, 2012.

7. Uber Technologies Inc. Uber elevate: Fast-forwarding to a future of on-demand urban air transportation. Technical report, Uber Technologies Inc., 2016.

8. A. Brown and W. Harris. A vehicle design and optimization model for on-demand aviation. In *2018 AIAA/ASCE/AHS/ASC Structures, Structural Dynamics, and Materials Conference, AIAA SciTech Forum*, Kissimmee, Florida, 2018. AIAA. Paper presented at the 2018 AIAA SciTech Forum.

9. Darli Rodrigues Vieira, Dreyfus Silva, and Alencar Bravo. Electric vtol aircraft: the future of urban air mobility (background, advantages and challenges). *International Journal of Sustainable Aviation*, 5(2):101–118, 2019.

10. Wayne Johnson, Christopher J. Silva, and Eduardo Solis. Concept vehicles for vtol air taxi operations. 2018.

11. Christopher Silva, Wayne R. Johnson, Eduardo Solis, Michael D. Patterson, and Kevin R. Antcliff. Vtol urban air mobility concept vehicles for technology development. *2018 Aviation Technology, Integration, and Operations Conference*, 2018.

12. Zhongqi Jia and Seongkyu Lee. Acoustic analysis of a quadrotor evtol design via high-fidelity simulations. In *25th AIAA/CEAS aeroacoustics conference*, page 2631, 2019.

13. Simone Albonico. Preliminary design of the anechoic wind tunnel of the department of aerospace science and technology of politecnico di milano. Master's thesis, Politecnico di Milano, 2024.

14. G. Bucherelli, L. Das, D. Granata, and A. Zanotti. Mid-fidelity numerical investigation of the interactional aerodynamic mechanisms in an electrical vertical take-off and landing quad-rotor aircraft. *Physics of Fluids*, 37(067138), 2025.

15. Daniel Weitsman, James H Stephenson, and Nikolas S Zawodny. Effects of flow recirculation on acoustic and dynamic measurements of rotary-wing systems operating in closed anechoic chambers. *The Journal of the Acoustical Society of America*, 148(3):1325–1336, 2020.

16. James H Stephenson, Daniel Weitsman, and Nikolas S Zawodny. Effects of flow recirculation on unmanned aircraft system (uas) acoustic measurements in closed anechoic chambers. *The Journal of the Acoustical Society of America*, 145(3):1153–1155, 2019.

17. J. Yin, F. De Gregorio, K.S. Rossignol, L. Rottmann, G. Ceglia, G. Reboul, G. Barakos, G. Qiao, M. Muth, M. Kessler, et al. Acoustic and aerodynamic evaluation of dlr small-scale rotor configurations within garteur ag26. In *Proceedings of the 49th European Rotorcraft Forum*, Bückeburg, Germany, September 2023. 5–7 September 2023.

18. Manuel Iannotta, Antonio Visingardi, Domenico Quagliarella, Fabrizio De Gregorio, Mattia Barbarino, and Alex Zanotti. Improvement of a free-wake model for the aerodynamic and aeroacoustic analysis of a small-scale two-bladed propeller in hover. *Aerospace*, 12(1), 2025.

19. Stewart Glegg and William Devenport. *Aeroacoustics of Low Mach Number Flows: Fundamentals, Analysis, and Measurement*. Elsevier Academic Press, London, UK, 2017.

20. Daniele Granata, Alberto Savino, Donato Grassi, Luca Riccobene, and Alex Zanotti. Aerodynamic and aeroacoustics investigation of tandem propellers in hover for evtol configurations. *Aerospace Science and Technology*, 155:109740, 2024.

21. N. S. Zawodny, D. D. Boyd Jr, and C. L. Burley. Acoustic characterization and prediction of representative, small-scale rotary-wing unmanned aircraft system components. In *American Helicopter Society (AHS) Annual Forum*, number NF1676L-22587, 2016.

CLASSIFICATION & COPYRIGHT